Time dependent interface stability during rapid solidification

K. Greven,[a] A. Ludwig, and P. R. Sahm
Giesserei-Institut der RWTH Aachen, 52056 Aachen, Germany

(Received 22 March 1999; accepted for publication 7 July 1999)

The destabilization of a planar solid/liquid interface during resolidification of the molten surface layer of Si–Sn alloys is investigated. Experimental data are compared with the results of a transient numerical stability analysis. In that analysis the time evolution of an infinitesimal sinusoidal perturbation of a planar interface is investigated. For this the concentration profile in the melt as well as the temperature distributions in the melt and solid are divided into a base state and a state due to the perturbation. The highly nonuniform Sn profiles implanted in (100) silicon samples serve as initial conditions for the numerical calculations. Deviations from thermal equilibrium at the solid/liquid interface are considered. The critical concentration for breakdown is calculated as a function of solidification velocity and compared with the results of the analytical analysis of Huntley and Davis [Acta Metall. Mater. **41**, 2025 (1993)]. It is further investigated whether an analytical steady-state stability analysis can be used to approximately describe the experiments considered.
 [S0021-8979(99)00620-9]

I. INTRODUCTION

Since the early 1950s many attempts have been made to describe the stability of a planar solid/liquid interface during alloy solidification. The first quantitative description was the constitutional supercooling criterion of Tiller *et al.*[1] Later Mullins and Sekerka[2] performed a linear stability analysis (known as MS analysis) by introducing an infinitesimal perturbation on a planar interface and considering the effect of surface tension. In both models local equilibrium at the interface was assumed. For nondilute alloys they got similar solutions for the limiting solidification velocity for planar growth, V_C, the constitutional supercooling limit.[3]

In contrast to Tiller *et al.*'s work, Mullins and Sekerka predicted restabilization of the planar solid/liquid interface at high growth rates. The limiting velocity for this phenomenon is called the absolute stability limit, V_{abs}. For velocities above this limit the solute diffusion distance is smaller than the capillary length. Thus, surface tension becomes dominant and wipes out all perturbations. As opposed to the constitutional supercooling limit, the absolute stability limit decreases with decreasing alloy concentration, which means that with decreasing concentrations V_C and V_{abs} approach each other and finally become unified at C^*.[4] Alloys with a concentration below C^* always grow with a stable planar solid/liquid interface.

Huntley and Davis[5] (HD) analysis extended the model of Mullins and Sekerka by taking into account deviations from the local equilibrium at the interface which become significant at high solidification velocities. They assumed that the partitioning coefficient changes with velocity as $k_V = \{(V/V_D)+k_e\}/\{(V/V_D)+1\}$, where k_e is the equilibrium distribution coefficient and V_D is the diffusion velocity across the interface.[6] In addition, they assume that the "effective" liquidus slope changes with velocity according to the expression given by Boettinger and Coriell.[7] Because they investigated not only spatial but also temporal perturbations, they revealed information on morphological and oscillatory instabilities. The latter are not of relevance for this article since they became important at solidification velocities greater than the 3–4 m/s occurring in the experiments considered.

The above mentioned analytical stability analyses assume that the solidification takes place under steady-state conditions. Besides a constant growth velocity (and in directional solidification besides a constant temperature gradient) a sufficiently large melt reservoir of uniform composition is necessary to enable the establishing of an exponential boundary layer ahead of the interface. If one of the steady-state conditions is not fulfilled, an analytical stability analysis cannot be applied and the problem must be solved numerically. Corriell *et al.*[8] calculated numerically the transient (one-dimensional) profile ahead of an infinitesimal perturbed planar solid/liquid interface which arises in the early stage of a Bridgman process. They used this transient profile to perform a linear stability analysis similar to that of Mullins and Sekerka. Ludwig *et al.*[9] used the same technique to investigate the destabilization of a planar solid/liquid interface subject to rapid quenching.

In this article a numerically calculated transient stability analysis is compared with the results of experiments on silicon–tin alloys, where a pulsed laser was used to melt a surface layer of the samples, which then resolidifies with large growth rates. These experiments were performed by a group at Harvard University.[10,11] They implanted ^{120}Sn in wafers of (100) Si and made the corresponding profiles of four differently processed samples available to us (see Fig. 1). A surface layer of the samples was melted with a pulse of a XeCl excimer laser (308 nm, pulse duration about 30 ns) which causes a maximum melt depth between 2000 and 4500

[a]Electronic mail: k.greven@gi.rwth-aachen.de

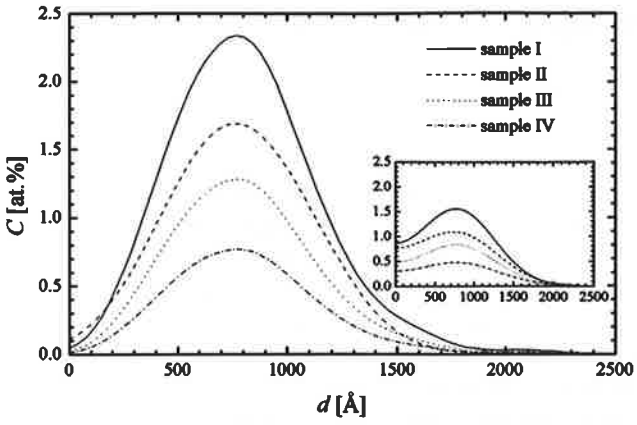

FIG. 1. Implanted Sn concentration as a function of depth for the four samples considered I–IV (see Table III) (taken from Ref. 11). The inset shows the calculated concentration profiles as they occur after complete melting of the surface layer. These profiles are input for the numerical stability analysis.

Å . After resolidification they measured the position at which the interface breakdown had taken place using a so called ion-channeling technique described in detail by Hoglund.[11] The concentration at the position of breakdown is then called the "interfacial solid concentration at breakdown," $C^*_{S,\mathrm{dest}}$.

By performing heat flow simulations they found that the solidification growth rate, V, as well as the temperature gradient in the liquid, G_L, can be considered constant.[10] The corresponding values for V and G_L together with the measured $C^*_{S,\mathrm{dest}}$ are listed in Table I. In addition to those constant quantities, there are three facts that are in contradiction to the steady-state conditions necessary for an analytical stability analysis: (i) the concentration profile after complete melting is not uniform (see the inset of Fig. 1), (ii) a solute pileup first has to be established in the early stages of solidification and (iii) the molten surface layer is of finite size, which means the influence of the sample boundary must be considered.

II. THEORETICAL MODEL

The linear stability analysis presented follows the work of Mullins and Sekerka.[2] Since the fact that any arbitrary perturbed interface can be described by a Fourier series, they considered the solidification front as a superposition of a planar front and an infinitesimal sinusoidal perturbation. By considering this the concentration and temperature fields can each be described as a linear superposition of a base state and a perturbation. For a solidification front growing under steady-state conditions Mullins and Sekerka derived an expression for the perturbation growth rate $\dot{\delta}/\delta$. If $\dot{\delta}/\delta$ is negative for all perturbation wavelengths λ, the planar interface is said to be stable; if it is positive for at least one λ, the interface is said to be unstable. For situations where the solidification takes place under nonsteady-state conditions as it does in the experiments considered, the whole set of equations has to be solved numerically. The course of the procedure for such an analysis is described in the following.

TABLE I. Experimentally measured values of melt depth $d_{\max}$, solidification velocity V, interfacial solid concentration at breakdown $C^*_{S,\mathrm{dest}}$ and the numerically estimated temperature gradient in the liquid G_L for the samples considered (taken from Ref. 11). The corresponding implanted Sn-concentration distributions and the profiles after melting are shown in Fig. 1.

Sample	$d_{\max}$ (Å)	V (m/s)	$C^*_{S,\mathrm{dest}}$ (at. %)	G_L (K/m)
I	2000	4.4	1.05	2.0×10^5
II	4500	3.1	0.60	2.0×10^5
III	2300	3.9	0.43	2.0×10^5
IV	3500	3.2	0.28	2.0×10^5

We consider a frame of reference moving with the solidification velocity V in the z direction, so that the planar solid/liquid interface remains at the origin of the coordinate system. The solute field in the melt $C(x,z,t)$ and the temperature fields in both the melt and the solid, $T_L(x,z,t)$ and $T_S(x,z,t)$, must satisfy the partial differential equations

$$\frac{\partial C}{\partial t}=V\frac{\partial C}{\partial z}+D\nabla^2 C,$$
$$\frac{\partial T_L}{\partial t}=V\frac{\partial T_L}{\partial z}+a_L\nabla^2 T_L, \tag{1}$$
$$\frac{\partial T_S}{\partial t}=V\frac{\partial T_S}{\partial z}+a_S\nabla^2 T_S.$$

Here, D is the solute diffusion coefficient and a_L and a_S are the thermal diffusivities of the melt and the solid, respectively. Diffusion in the solid is neglected. Considering an infinitesimal perturbation of the form of $\delta(t)\sin(\omega x)$, with wave number $\omega=2\pi/\lambda$, the solute and thermal flux balance at the maximum amplitude are given by

$$v(1-k_v)C|_{z=\delta}=-D\left.\frac{\partial C}{\partial z}\right|_{z=\delta}, \tag{2}$$

$$\Delta H\cdot v=\lambda_S\left.\frac{\partial T_S}{\partial z}\right|_{z=\delta}-\lambda_L\left.\frac{\partial T_L}{\partial z}\right|_{z=\delta}, \tag{3}$$

with the latent heat of fusion per unit volume being ΔH, the thermal conductivity of the melt λ_L and the solid λ_S. The growth velocity at $z=\delta$ results from $v=V+\dot{\delta}$. If the deviation from thermodynamic equilibrium is accounted for by the formalism described by Boettinger and Coriell[7] (where an "effective" liquidus slope m_V is introduced) the curvature can be considered by

$$T_L|_{z=\delta}=T_S|_{z=\delta}=T_M+m_V C|_{z=\delta}-\Gamma\omega^2\delta, \tag{4}$$

with the melting point of the pure solvent being T_M and the Gibbs-Thomson coefficient Γ.

In the next step all profiles are written as the superposition of a base state $C^{\mathrm{base}}(z,t)$, $T_L^{\mathrm{base}}(z,t)$, $T_S^{\mathrm{base}}(z,t)$ and a perturbation $C^{\mathrm{pert}}(z,t)\sin(\omega x)$, $T_L^{\mathrm{pert}}(z,t)\sin(\omega x)$, $T_L^{\mathrm{pert}}(z,t)\sin(\omega x)$, each of which satisfies Eq. (1). Performing a Taylor expansion at $z=\delta$ and neglecting all terms of second or higher order, Eqs. (2)–(4) can be separated into corresponding expressions for the base state and the perturbations.

For the base state this leads to the well known boundary conditions for an unperturbed flat interface:

$$V(1-k_V)C^{\text{base}}|_{z=0} = -D\left.\frac{\partial C^{\text{base}}}{\partial z}\right|_{z=0}, \tag{5}$$

$$\Delta H \cdot V = \lambda_S \left.\frac{\partial T_S^{\text{base}}}{\partial z}\right|_{z=0} - \lambda_L \left.\frac{\partial T_L^{\text{base}}}{\partial z}\right|_{z=0}, \tag{6}$$

$$T_L^{\text{base}}|_{z=0} = T_S^{\text{base}}|_{z=0} = T_M + m_V C^{\text{base}}|_{z=0}. \tag{7}$$

The base states of the temperature distribution in the melt and the solid are assumed to be linear which is a justified approximation for the experiments considered. With the temperature gradient in the liquid known, the temperature gradient in the solid can then be determined using Eq. (6), while Eq. (5) serves as a boundary condition for the numerical estimation of the base state of the concentration profile.

For the temperature and concentration fields of the perturbation the following set of equations is obtained:

$$V(1-k_V)\left(C^{\text{pert}}|_{z=0} + \delta \cdot \left.\frac{\partial C^{\text{base}}}{\partial z}\right|_{z=0}\right) + \dot{\delta}(1-k_V)C^{\text{base}}|_{z=0}$$
$$= -D\left(\left.\frac{\partial C^{\text{pert}}}{\partial z}\right|_{z=0} + \delta \left.\frac{\partial^2 C^{\text{base}}}{\partial z^2}\right|_{z=0}\right), \tag{8}$$

$$\Delta H \cdot \dot{\delta} = \lambda_S \left(\left.\frac{\partial T_S^{\text{pert}}}{\partial z}\right|_{z=0} + \delta \left.\frac{\partial^2 T_S^{\text{base}}}{\partial z^2}\right|_{z=0}\right)$$
$$- \lambda_L \left(\left.\frac{\partial T_L^{\text{pert}}}{\partial z}\right|_{z=0} + \delta \left.\frac{\partial^2 T_L^{\text{base}}}{\partial z^2}\right|_{z=0}\right), \tag{9}$$

$$T_L^{\text{pert}}|_{z=0} + \delta \left.\frac{\partial T_L^{\text{base}}}{\partial z}\right|_{z=0} = T_S^{\text{pert}}|_{z=0} + \delta \left.\frac{\partial T_S^{\text{base}}}{\partial z}\right|_{z=0}$$
$$= m_V \left(C^{\text{pert}}|_{z=0} + \delta \left.\frac{\partial C^{\text{base}}}{\partial z}\right|_{z=0}\right)$$
$$- \Gamma \omega^2 \delta. \tag{10}$$

Here it is assumed that $k_v \approx k_V$ and $m_v \approx m_V$ which seems to be justified as the change of both quantities with velocity is small.

The four equations, (8)–(10), represent a system of linear equations which serve as boundary conditions for the numerical estimation of the three perturbation profiles and the growth rate $\dot{\delta}/\delta$. They are solved in an iterative way. All perturbation fields are calculated with a vanishing gradient at the end of the numerical domain. The initial solute profile of the base state was calculated from the implanted profile by simulating the melting process (see Fig. 1). The initial perturbation profiles were taken to be zero.

To formulate the numerical algorithm, the differential equations are spatially discretized with second order accuracy on a uniform mesh in the spatial variable z. During melting of the sample and the solidification process that follows a numerical domain with variable length is considered. The differential equations were solved in a fully implicit way. The thermodynamical data used for the numerical simulation are shown in Table II. Interface breakdown is assumed as soon as one λ exists with a positive $\dot{\delta}/\delta$. Thus the time for breakdown is given by the minimum in the t_{dest}-λ curve. The corresponding interfacial solid concentration defines $C^*_{S,\text{dest}}$.

TABLE II. Thermodynamic data of silicon–tin used for the numerical calculation.

Quantity	Symbol	Value
Diffusivity of tin in liquid silicon	D	2.5×10^{-8} m^2/s[a]
Diffusion velocity	V_D	17 m/s[a]
Thermal conductivity of the liquid at T_M	λ_L	140 W/(mK)[b]
Thermal conductivity of the solid at T_M	λ_S	22.0 W/(mK)[b]
Melting temperature of pure silicon	T_M	1685 K[c]
Equilibrium partition coefficient	k_e	0.016[d]
Equilibrium liquidus slope	m_e	−4.6 K/at. %
Surface tension	γ	0.45 J/m^2[e]
Latent heat of fusion per unit volume	ΔH	4.19×10^9 J/m^3[f]

[a]Reference 11.
[b]Reference 12.
[c]Reference 13.
[d]Reference 14.
[e]Reference 15.
[f]Reference 16.

III. RESULTS AND DISCUSSION

The Sn profiles prior to solidification are shown in the inset of Fig. 1. As stated above they were estimated by simulating the melting of the surface layer during the laser treatment. Although a broadening of the implanted profiles due to diffusion in the liquid occurs during the melting procedure, the Sn concentration still reveals a marked maximum in all four cases. These profiles are taken as an initial solute distribution for the stability analysis.

For sample I the calculated concentration profile of the base state at the predicted moment of interface breakdown is shown in Fig. 2 (solid line). The rectangles show the measured concentration profile in the solidified sample. On the left-hand side of the solute pile up the concentration profile in the melt and in the final solid cannot be compared. On the right-hand side of the concentration pileup the agreement between the calculated concentration profile in the solid and the measurement is good.

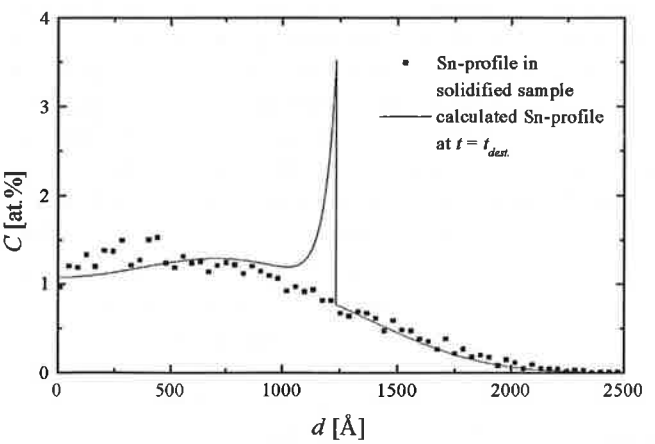

FIG. 2. Calculated Sn distribution in sample I at the moment predicted for interface breakdown (solid line). The rectangles represent the measured concentration distribution in the solidified sample.

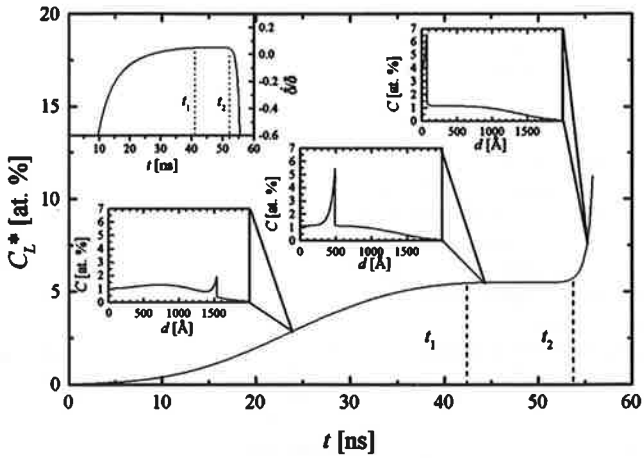

FIG. 3. Interfacial liquid concentration as function of time (sample I) showing the three different stages of solidification. The insets show the concentration distribution in the sample at different times. The evolution of the perturbation growth rate with time for one certain wavelength λ is shown in the upper left inset.

In Fig. 3 the calculated interfacial concentration in the melt C_L^* (base state) of sample I is shown as a function of time together with three representative concentration profiles at different solidification process times (insets). All curves in Fig. 3 are calculated by assuming a planar solidification throughout the whole sample although after a certain time $\dot{\delta}/\delta$ becomes positive for a certain range of λ. However, Fig. 3 gives a clue as to the transient nature of this solidification process. Together with the result of the stability analysis, such calculations can predict whether or not a quasisteady state can be established before interface breakdown occurs.

From Fig. 3 it becomes obvious that the solidification process can be divided into three stages. The first one is a transient stage characterized by the strong time dependence of the interfacial liquid concentration. During that stage the concentration profile within the melt is very different from a steady-state profile. The solute pileup is yet not fully established and there is still a remarkable concentration profile ahead of the developing boundary layer (see the corresponding inset). After a certain time t_1 the interfacial liquid concentration becomes independent of time which means the solidification front has reached a quasisteady state. The concentration profile ahead of the boundary layer has completely flattened due to diffusion and there is not yet any influence of the sample surface on the concentration field. At time t_2 a steep increase of the interfacial concentration with time occurs due to interaction of the concentration field with the sample boundary. These three stages of solidification can also be seen in the plot of the time evolution of the perturbation wavelength $\dot{\delta}/\delta$, as is shown for one certain wavelength in the upper left inset in Fig. 3: $\dot{\delta}/\delta$ increases for $t \leqslant t_1$, it can be regarded to be constant for $t_1 \leqslant t \leqslant t_2$ and it decreases again for $t_2 \leqslant t$. It is obvious that interface breakdown must occur during the development of the solute pileup in the transient stage of solidification [stage (i)].

Table III shows the times of both of these transitions, t_1 and t_2, for all the samples. Keeping in mind the assumption made during the derivation of an analytical stability analysis,

TABLE III. Times that indicate the beginning and the end of quasisteady-state solidification, t_1 and t_2, respectively, together with calculated values concerning the interface breakdown (destabilization time t_{dest}, interfacial solid concentration at breakdown $C^*_{S,dest}$ and perturbation wavelength λ_{min}).

Sample	t_1 (ns)	t_2 (ns)	t_{dest} (ns)	$C^*_{S,dest}$ (at. %)	λ_{min} (nm)
I	40	52	25.8	0.77	90
II	110	130	105.5	0.39	164
III	56	65	45.5	0.49	125
IV	112	117	93.9	0.30	135

it is obvious that such an analysis is only suitable to describe the experiments considered within the time interval $t_1 \leqslant t \leqslant t_2$. This is discussed in more detail below.

Figure 4 shows the time of destabilization, t^{λ}_{dest}, and the interfacial solid concentration $C^{*,\lambda}_{S,dest}$ at the moment of interface breakdown as a function of the perturbation wavelength λ. The appearance of a minimum is the result of two wavelength-dependent stabilizing effects. For small perturbation wavelengths the surface tension is dominant and it tends to flatten the interface, while for long wavelengths the positive temperature gradient in the liquid hinders the perturbation from growing. Since interface breakdown is assumed if at least one perturbation wavelength is unstable, the minimum in the t^{λ}_{dest}-λ curve in Fig. 4 provides the time, t_{dest}, and the interfacial solid concentration, $C^*_{S,dest}$ of interface breakdown. These values and those related to the perturbation wavelength, λ_{min}, are shown in Table III.

To compare the time-dependent numerical stability analysis presented with the analytical analysis of Huntley and Davis, the interfacial solid concentration for breakdown was calculated as a function of solidification velocity assuming a constant temperature gradient in the melt, specified in Table I. Since it is not possible to consider the influence of the initial transient, the finite sample size or a nonuniform initial solute profile in an analytical analysis, the HD analysis predicts that the four experimentally determined $C^*_{S,dest}$ are described by one single $C^*_{S,dest}$-V curve. If this analysis would hold to describe the experimentally observed interface breakdown the measured $(C^*_{S,dest}, V)$ pairs should lie on that curve. As shown in Fig. 5, only two of the four experimental

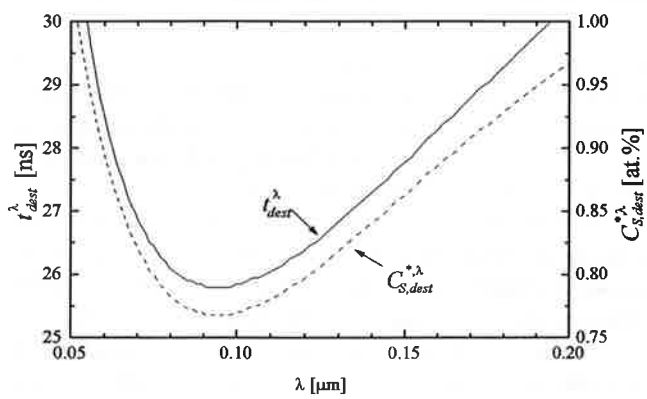

FIG. 4. Interface concentration in the solid at the moment of breakdown $C^*_{S,dest}$ (solid line) and the time interval which is needed for interface breakdown t^{λ}_{dest} (dashed line) as a function of the perturbation wavelength.

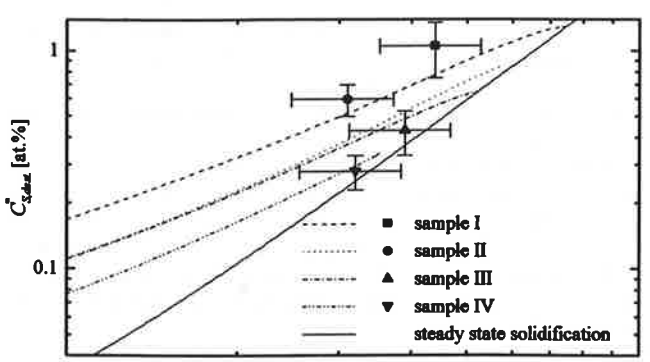

FIG. 5. Interfacial solid concentration for breakdown for both the numerical and the analytical (steady-state) analysis. The experimental results of each sample are shown by the symbols.

points hit the theoretical prediction of the HD analysis. It can be seen in Table III that these two samples are the ones with the smallest deviation between t_{dest} and t_1. This means that the quasisteady-state [stage (ii)] of the solidification has almost been reached and that the steady-state analysis represents a good approximation with which to describe the measurements.

In contradiction to the HD analysis, the numerical stability analysis predicts a different $C^*_{S,\mathrm{dest}}$-V curve for each experiment due to differences in melt depths and initial concentration distributions. From Fig. 5 it is obvious that all numerical results predicts larger $C^*_{S,\mathrm{dest}}$ than the analytical model. This deviation gets more decisive for those samples which show the largest difference between t_{dest} and t_1.

Another striking difference is that the numerical result predicts no morphological destabilization of the interface at all above a certain velocity. The reason for that is the finite size of the sample. As it can be seen in the upper left inset in Fig. 3, the perturbation growth rate starts at negative values, increases to its steady-state value and decreases again as soon as the boundary layer approaches the sample surface. Above a certain velocity there is not enough time for the solid/liquid interface to develop a concentration gradient steep enough to destabilize the interface before the concentration boundary layer approaches the sample surface. Under such conditions the solidification process is fully transient: The boundary layer reaches the sample surface before the solute pileup ahead of the interface is fully developed.

The comparison between the numerical results and the experimental measurements (Fig. 5) shows reasonable agreement. It can be seen that the experimental results of all samples, except that of sample II, are hit by the concerning numerical curve within the error of measurement. The deviation between simulation and experiment for sample II may be caused by insufficient knowledge about the implanted Sn profile. The error bars at the experimental values are estimated from the uncertainty of the concentration measurements and that of the heat flow calculation, made to determine V and G_L.[11] The latter source of error also contributes to the uncertainty of the simulation results, since V and G_L, both results of the heat flow calculation, are input for the numerical stability analysis. Further uncertainties of the numerical results result from the uncertainty of the initial conditions, e.g., the concentration profile prior to solidification and the thermodynamic and material specific data, e.g., diffusion coefficient, V_D, etc.

IV. SUMMARY AND CONCLUSIONS

A time-dependent numerical stability analysis of a solid/liquid interface was performed by investigating the time evolution of an infinitesimal harmonic perturbation considering (i) the establishing of a solute pileup ahead of the interface, (ii) a nonuniform initial solute profile in the melt and (iii) a finite sample size. The temperature profiles in the solid and liquid as well as the concentration profile ahead of the interface are divided into a base state and a state due to the perturbation. The base state of the concentration profile C^{base} as well as the perturbation fields C^{pert}, T_L^{pert} and T_S^{pert} are calculated numerically and the moment of morphological breakdown of the initially planar interface is estimated. The corresponding interfacial solid concentration is compared with experimental results. The following conclusions can be drawn.

(1) Resolidification of the molten layer can be divided into three stages: (i) the initial transient where a solute pileup ahead of the interface is established, (ii) a quasisteady-state growth where the interfacial concentration remains almost constant and the concentration field ahead of the boundary layer became uniform due to diffusion in the liquid and (iii) a steep increase in the interfacial concentrations when the boundary layer reaches the sample surface.
(2) If destabilization of the solid/liquid interface takes place it must happen during stage (i), the establishing of the solute pileup.
(3) If the solid/liquid interface remains planar during the whole solidification process, no quasisteady-state growth occurs. The establishing of the solute pileup is directly followed by interaction of the boundary layer with the sample surface. This happens above a defined velocity limit.
(4) It is shown that analytical analysis has to be used carefully for interpretation of the experimental data, since interface breakdown takes place during the initial transient stage of solidification. In at least two cases of the experimental data shown, the assumption of steady state turns out to be not a good approximation.
(5) With regard to the reasonable agreement between predictions and the experimental results, the time-dependent numerical stability analysis performed seems to be a proper method by which to interpret the experimental data.

ACKNOWLEDGMENTS

The authors would like to thank Professor M. J. Aziz and Dr. D. Hoglund of Harvard University for making detailed experimental information available. This research was done within the framework of the "Graduiertenkolleg: Schmelzen, Erstarrung und Grenzflächen" of RWTH Aachen and DLR

Cologne, and was sponsored by the German Science Foundation whom the authors kindly acknowledge.

[1] W. A. Tiller, K. A. Jackson, J. W. Rutter, and B. Chalmers, Acta Metall. **1**, 428 (1953).
[2] W. W. Mullins and R. F. Sekerka, J. Appl. Phys. **35**, 444 (1964).
[3] W. Kurz and D. J. Fisher, *Fundamentals of Solidification* (Trans Tech, Aedermannsdorf, Switzerland, 1992).
[4] C^* depends on the interfacial temperature gradient.
[5] D. A. Huntley and S. H. Davis, Acta Metall. Mater. **41**, 2025 (1993).
[6] M. J. Aziz, J. Appl. Phys. **53**, 1158 (1982).
[7] W. J. Boettinger and S. R. Coriell, in *Science and Technology of the Undercooled Melt: Rapid Solidification of Materials and Technologies*, edited by P. R. Sahm, H. Jones, and C. M. Adam (Nijhoff, Dordrecht, 1986), p. 81.
[8] S. R. Coriell, R. F. Boisvert, G. B. McFadden, L. N. Brush, and J. J. Favier, J. Cryst. Growth **140**, 139 (1994).
[9] A. Ludwig, K. Greven, and P. R. Sahm, J. Cryst. Growth **186**, 291 (1998).
[10] D. E. Hoglund, M. J. Aziz, S. R. Stiffler, M. O. Thompson, J. Y. Tsao, and P. S. Peercy, J. Cryst. Growth **109**, 107 (1991).
[11] D. E. Hoglund, Interface Stability During Rapid Solidification of Silicon-Tin, Ph.D. thesis, Harvard University, 1996.
[12] C. Y. Ho, R. W. Powell, and P. E. Liley, *Thermal Conductivity of the Elements: A Comprehensive Review* (American Chemical Society, Washington, 1971).
[13] *Selected Values of the Thermodynamic Properties of the Elements*, edited by R. Hultgren, P. D. Desai, D. T. Hawkins, M. Gleiser, K. K. Kelley, and D. D. Wagman (American Society for Metals, Metals Park, OH, 1973).
[14] C. D. Thurmond and M. Kowalchik, Bell Syst. Tech. J. **39**, 169 (1960).
[15] Y. Shao and E. Spaepen, J. Appl. Phys. **79**, 2981 (1996).
[16] Y. S. Touloukian, *Thermophysical Properties of Matter: The Thermophysical Properties Research Center Data Series* (IFI/Plenum, New York, 1970–1979).